

# Recognized Maritime Picture: Geofeasibility Scores

Mark Coates

*Coordinator, McGill University*

Marie-Odette St-Hilaire

*Industrial representative, Lockheed Martin Canada*

Nando de Freitas

*Professor, University of British Columbia*

Francis Moreau

*Student, Université de Montréal*

Boris Oreshkin

*Student, McGill University*

Mary Pugh

*Professor, University of Toronto*

## 1. Introduction

Maritime security is a considerable challenge for Canada due to its extensive coastline (150,000 miles) and its vast area of responsibility (over 6.7 million square miles). There are 250 ports in Canada and between 1500 and 2000 reported ships in its area of responsibility [3]. It may be the case that many ships do not self-report because they are far from port and not covered by the vessel traffic management system.

A Recognized Maritime Picture (RMP) is a plot compiled to depict maritime activity. The term “recognized” means that the picture has been evaluated prior to its distribution. A central authority compiles and fuses the data from many stations and evaluates their validity. The construction of an RMP consists of detecting objects of interest (ships), classifying them, assessing what they are doing, and deciding whether any type of follow-on action is required [9].

The Canadian Department of National Defense receives data from numerous sensor and information systems, operated by both civilian and military authorities. These systems include automatic self-reporting positional systems, air patrol surveillance systems, high frequency surface radars, electronic intelligence systems, radar space systems, and high frequency direction finding sensors [9]. One of the primary challenges of the Department is fusing the data from all of these sources, whilst trying to make full, accurate use of the information in a timely fashion.

Human operators are a key component of the current fusion system, but they are overloaded. There is insufficient automation in the system, resulting in inadequate fusion of the data, and the integration is relatively poor. The human operators are presented with too much information and must make too many decisions, a fact that significantly reduces the efficacy of the system. The result is that the initial version of the RMP is overloaded with multiple tracks, derived from different sources and sensor systems, that represent the same ship. The operators must decide whether two tracks are generated by the same ship, basing their decision on ship attributes and geographic considerations. It is highly desirable that this process be partially automated, so that the human operators have to make assessments about borderline cases only.

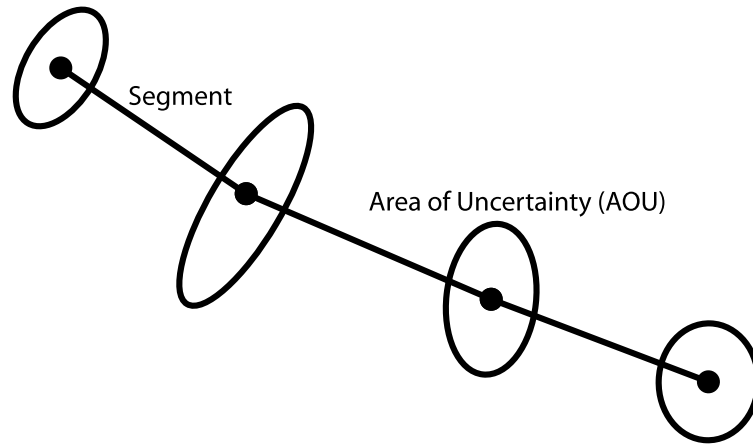


Figure 1. An example track showing the  $2\sigma$  areas of uncertainty derived at each time instant

In each report, a source associates an area of uncertainty (AOU) of elliptic shape to a ship, delimiting a  $2\sigma$  probability region (corresponding to a Gaussian distribution). Figure 1 depicts an example track. During the workshop, we considered the problem of reaching decisions based solely on geographic considerations. Our goal was to derive metrics that reflect the probability that two tracks are generated by the same ship (based solely on geographic considerations). A metric, or geofeasibility score  $g$ , must have a value comprised between zero and one, with a higher value representing a greater probability that the tracks are generated by the same ship. There are three basic constraints on the function  $g$ :

$$g(x) \in [0, 1], \quad (46)$$

$$g(x) = 0 \quad \text{if ellipses do not touch, and} \quad (47)$$

$$g(x) = 1 \quad \text{if ellipses overlap totally.} \quad (48)$$

In this report, we focus on the generation of a geofeasibility score based on a single, common time instant. This score is based solely on the ellipses and the underlying Gaussian distributions. In practice, multiple such geofeasibility scores would be combined (probably by using a harmonic or geometric mean) in order to derive a total score for the tracks.

We now discuss briefly the interest of Lockheed Martin Canada in the present work. The Research and Development Department of Lockheed Martin Canada was part of the DRDC Multi-Sensor Integration within a Common Operating Environment (MUSIC) Technical Demonstration Project [8]. As part of this project, a team of government and contract researchers developed a track fusion application that is expected to be fielded in the Canadian Navy's operation centers within the current year. Geofeasibility scoring plays an important part in the track-to-track fusion system developed within the MUSIC project for two main reasons: the score is evaluated a huge number of times (benchmark: 100,000 score evaluations per hour) and is visualized by operators on the RMP. Because of the second reason, the score must be intuitive enough for an operator to understand it, and therefore trust it. The descriptions of the track modeling approach and the track-to-track fusion process can be found in [10] and [5], respectively.

## 2. Proposed Solutions

### 2.1. SELECTED METRIC

We select as a metric the normalized overlap area between two ellipses, which can be defined as follows:

$$g = \frac{\int \mathbf{1}_{\{\mathbf{x} \in \mathcal{S}_1 \cap \mathcal{S}_2\}} d\mathbf{x}}{\int \mathbf{1}_{\{\mathbf{x} \in \mathcal{S}_{\min}\}} d\mathbf{x}}, \quad (49)$$

where the numerator is the area of the intersection between the ellipses defined by regions  $\mathcal{S}_1$ ,  $\mathcal{S}_2$ , and  $\mathcal{S}_{\min}$  is the ellipse having the smallest area:

$$\mathcal{S}_{\min} \triangleq \arg \min_{\mathcal{S}_1, \mathcal{S}_2} \left[ \int \mathbf{1}_{\{\mathbf{x} \in \mathcal{S}_1\}} d\mathbf{x}, \int \mathbf{1}_{\{\mathbf{x} \in \mathcal{S}_2\}} d\mathbf{x} \right]. \quad (50)$$

Note that (49) satisfies the requirements for a metric.

### 2.2. MONTE-CARLO INTEGRATION

The direct calculation of (49) is not viable analytically because it is not possible to define the limits of integration in the numerator. The integration limits are defined by the intersection points of two ellipses and an analytical formula for the general case is not available. Some of the team members used Newton's method to try to compute the points of intersection between the two ellipses (see the presentation on the web site of the workshop). Here we discuss Monte-Carlo integration, a powerful tool that can be used to resolve problems of this kind. It is suitable for the computation of integrals having the following form:

$$I = \int \int \int_{\mathcal{S}} f(x_1, x_2, \dots, x_K) dx_1 dx_2 \dots dx_K, \quad (51)$$

where  $\mathcal{S}$  is the set of integration limits. Monte-Carlo integration is useful when the integral in (51) cannot be evaluated analytically for some reason, but  $f(x_1, x_2, \dots, x_K)$  can be evaluated pointwise. Moreover, the set of integration limits can be defined by a set of rules or otherwise evaluated in an efficient way during the execution of a numerical calculation routine. The simplest Monte-Carlo algorithm samples  $N$  random vectors  $\mathbf{x}^{(i)} = (x_1^i, x_2^i, \dots, x_K^i)^T$  (for  $i = 1, \dots, N$ ) uniformly from the volume defined by  $\mathcal{S}$  and approximates the integral (51) by the sum:

$$\hat{I} = \frac{1}{N} \sum_{i=1}^N f(\mathbf{x}^{(i)}). \quad (52)$$

The estimator (52) is unbiased [2]. Moreover, the variance of this estimator is shown to decay with the rate  $N$  [2], which means that (52) is a consistent estimator of (51) [7].

The direct application of the naive Monte-Carlo algorithm is limited by the fact that the integration volume  $\mathcal{S}$  itself is often hard to evaluate analytically. Thus a more general algorithm is commonly used. In this algorithm one defines a probability density  $p(\mathbf{x})$  that supports the volume of interest  $\mathcal{S}$  and is easy to sample from. The random vectors  $\mathbf{x}^{(i)}$  are now sampled from this density and the integral (51) can be easily represented as

$$I = \int \int \int_{-\infty}^{+\infty} \mathbf{1}_{\{\mathbf{x} \in \mathcal{S}\}} \frac{f(\mathbf{x})}{p(\mathbf{x})} p(\mathbf{x}) d\mathbf{x}, \quad (53)$$

where  $\mathbf{1}_{\{\cdot\}}$  is the Riemann kernel. The application of the importance sampling [2] paradigm results in an estimator of the following form:

$$\hat{I} = \frac{1}{N} \sum_{i=1}^N \mathbf{1}_{\{\mathbf{x}^{(i)} \in \mathcal{S}\}} \frac{f(\mathbf{x}^{(i)})}{p(\mathbf{x}^{(i)})}. \quad (54)$$

Thus we propose to estimate the value of the normalized overlap area metric (introduced above) by the following Monte–Carlo algorithm:

$$g_M = \frac{\sum_{i=1}^N \mathbf{1}_{\{\mathbf{x}^{(i)} \in \mathcal{S}_1 \cap \mathcal{S}_2\}} \frac{1}{p_{\mathcal{S}_{\min}}(\mathbf{x}^{(i)})}}{\sum_{i=1}^N \mathbf{1}_{\{\mathbf{x}^{(i)} \in \mathcal{S}_{\min}\}} \frac{1}{p_{\mathcal{S}_{\min}}(\mathbf{x}^{(i)})}}, \quad (55)$$

where the  $\mathbf{x}^{(i)}$  are samples drawn from the Gaussian distribution  $p_{\mathcal{S}_{\min}}(\mathbf{x})$  with parameters defined by the ellipse  $\mathcal{S}_{\min}$  having the smallest area. In general the  $2\sigma$  ellipse and corresponding  $\mathcal{S}$  can be parameterized by its semi-axes  $r_x, r_y$ , bearing angle  $\varphi$ , and translation of the center  $x_0, y_0$ . The mapping between the ellipse parameters and the parameters of the Gaussian distribution  $p_{\mathcal{S}}(\mathbf{x}) \triangleq \mathcal{N}(\mu, \mathbf{R})$  consists of the following two parts. Firstly, the covariance  $\mathbf{R}$  is connected to  $r_x, r_y$ , and  $\varphi$  by the following:

$$\mathbf{U} = \begin{bmatrix} \sin(\varphi) & \cos(\varphi) \\ \cos(\varphi) & -\sin(\varphi) \end{bmatrix} \quad (56)$$

$$\mathbf{\Lambda} = \begin{bmatrix} \frac{r_x^2}{4} & 0 \\ 0 & \frac{r_y^2}{4} \end{bmatrix} \quad (57)$$

$$\mathbf{R} = \mathbf{U}\mathbf{\Lambda}\mathbf{U}^T. \quad (58)$$

Secondly,  $\mu$  is connected to  $x_0, y_0$  by the following:

$$\mu_1 = x_0, \quad \mu_2 = y_0. \quad (59)$$

### 2.3. GENERALIZED LIKELIHOOD RATIO

In this section we describe an alternative metric. We assume that the source provides us with noisy measurements  $\mathbf{y}_1, \mathbf{y}_2$  of the true target coordinates  $\mu_1, \mu_2$ , and with Maximum Likelihood (ML) estimators of measurement covariance matrices  $\hat{\mathbf{R}}_1, \hat{\mathbf{R}}_2$ . We choose to construct a test statistic to discriminate between the two hypotheses:

$$H_1 : \mu_1 = \mu_2, \quad (60)$$

$$H_0 : \mu_1 \neq \mu_2. \quad (61)$$

It is known [7] that in this case a Uniformly Most Powerful test does not exist. However, we can resort to a suboptimum statistic that is called the Generalized Likelihood Ratio (GLR):

$$\Lambda(\mathbf{y}_1, \mathbf{y}_2) = \frac{\max_{\Theta} p(\mathbf{y}_1, \mathbf{y}_2 | \Theta, H_1)}{\max_{\Theta} p(\mathbf{y}_1, \mathbf{y}_2 | \Theta, H_0)}. \quad (62)$$

Here  $\Theta$  stands for the unknown parameters  $\mu_1, \mu_2, \mathbf{R}_1, \mathbf{R}_2$ . Given the Gaussian and independence assumptions on the underlying distribution  $p(\cdot)$ , we have

$$p(\mathbf{y}_1, \mathbf{y}_2 | \Theta, H) = \frac{1}{(2\pi)^2 \sqrt{\det(\mathbf{R}_1) \det(\mathbf{R}_2)}} \exp \left[ -\frac{1}{2} \left( (\mathbf{y}_1 - \mu_1)^T \mathbf{R}_1^{-1} (\mathbf{y}_1 - \mu_1) + (\mathbf{y}_2 - \mu_2)^T \mathbf{R}_2^{-1} (\mathbf{y}_2 - \mu_2) \right) \right]. \quad (63)$$

We deduce immediately that the following equation holds under  $H_0$ .

$$\max_{\Theta} p(\mathbf{y}_1, \mathbf{y}_2 | \Theta, H_0) = \frac{1}{(2\pi)^2 \sqrt{\det(\hat{\mathbf{R}}_1) \det(\hat{\mathbf{R}}_2)}} \quad (64)$$

On the other hand, to find the ML estimator of the mean under  $H_1$ , we use  $\mu \triangleq \mu_1 = \mu_2$  and equate the partial derivative to 0:

$$\frac{\partial}{\partial \mu} p(\mathbf{y}_1, \mathbf{y}_2 | \Theta, H_1) = \mathbf{R}_1^{-1} (\mathbf{y}_1 - \mu) + \mathbf{R}_2^{-1} (\mathbf{y}_2 - \mu) = 0. \quad (65)$$

This results in the following expression for the ML estimator of the mean.

$$\hat{\mu} = \left[ \mathbf{R}_1^{-1} + \mathbf{R}_2^{-1} \right]^{-1} \left[ \mathbf{R}_1^{-1} \mathbf{y}_1 + \mathbf{R}_2^{-1} \mathbf{y}_2 \right] \quad (66)$$

Substituting (64) and (66) into the likelihood ratio (62), we get the statistic of the form

$$\Lambda(\mathbf{y}_1, \mathbf{y}_2) = \exp \left( -\frac{1}{2} \Delta^T \hat{\mathbf{R}}_{\Delta}^{-1} \Delta \right), \quad (67)$$

where  $\Delta$  is the difference between the measurements:

$$\Delta = \mathbf{y}_1 - \mathbf{y}_2, \quad (68)$$

and the estimate of the covariance inverse is given by the formula

$$\begin{aligned} \hat{\mathbf{R}}_{\Delta}^{-1} &= \hat{\mathbf{R}}_2^{-1} \left[ \hat{\mathbf{R}}_1^{-1} + \hat{\mathbf{R}}_2^{-1} \right]^{-1} \hat{\mathbf{R}}_1^{-1} \left[ \hat{\mathbf{R}}_1^{-1} + \hat{\mathbf{R}}_2^{-1} \right]^{-1} \hat{\mathbf{R}}_2^{-1} \\ &\quad + \hat{\mathbf{R}}_1^{-1} \left[ \hat{\mathbf{R}}_1^{-1} + \hat{\mathbf{R}}_2^{-1} \right]^{-1} \hat{\mathbf{R}}_2^{-1} \left[ \hat{\mathbf{R}}_1^{-1} + \hat{\mathbf{R}}_2^{-1} \right]^{-1} \hat{\mathbf{R}}_1^{-1}. \end{aligned} \quad (69)$$

It is straightforward to show, by using the rule that the inverse of the product is equal to the product of the inverses (in reverse order), that the following holds:

$$\hat{\mathbf{R}}_{\Delta}^{-1} = \left[ \hat{\mathbf{R}}_1 + \hat{\mathbf{R}}_2 \right]^{-1}. \quad (70)$$

Hence the geofeasibility score based on GLR admits the following simple and intuitive form:

$$g_G = \exp \left( -\frac{1}{2} \Delta^T \left[ \hat{\mathbf{R}}_1 + \hat{\mathbf{R}}_2 \right]^{-1} \Delta \right). \quad (71)$$

Note that (71) does not satisfy the requirements for a metric. In Section 3, however, it will be argued that in most cases this issue can be resolved by using simple thresholding.

It is interesting to observe that (71) is closely related to the Mahalanobis distance, which is defined as follows [6]:

$$d(\mathbf{x}, \mathbf{y}) = \sqrt{(\mathbf{x} - \mathbf{y})^T \mathbf{Q}^{-1} (\mathbf{x} - \mathbf{y})}, \quad (72)$$

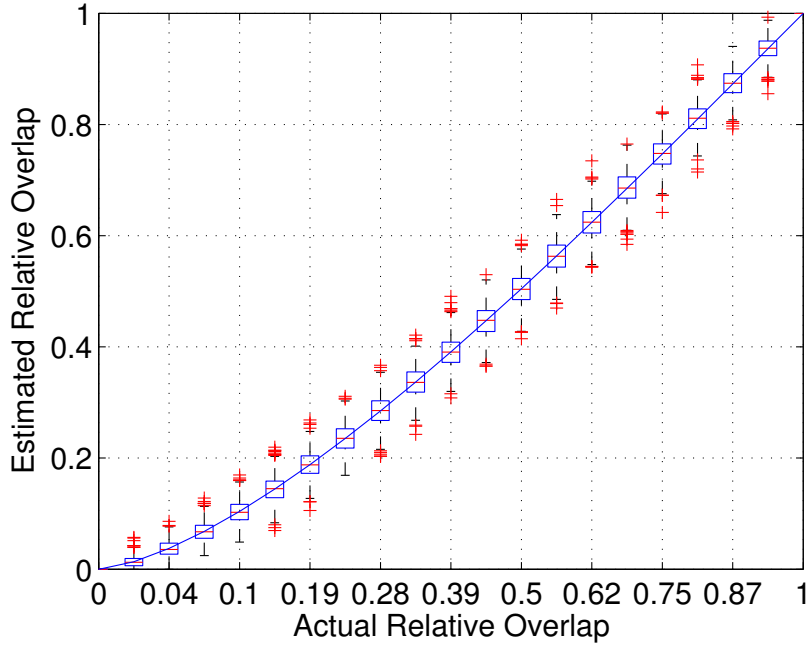


Figure 2. A comparison between the actual relative overlap and the estimated relative overlap using Monte–Carlo integration with number of samples  $N = 500$ . The line depicts the true value; the error bars are derived from 1000 trials of the Monte–Carlo integration technique. The scenario used to generate these results is the special case of overlapping circles, which is the only case where an analytical expression for the overlap can be derived.

and where it is assumed that  $\mathbf{x}$  and  $\mathbf{y}$  are jointly Gaussian random vectors drawn from the same distribution with covariance  $\mathbf{Q}$ . In our case  $\mathbf{Q}$  is unknown and we outline a statistical procedure (see (70)) that is used to estimate  $\mathbf{Q} \triangleq \hat{\mathbf{R}}_{\Delta}$  from the available data  $\hat{\mathbf{R}}_1$  and  $\hat{\mathbf{R}}_2$ .

### 3. Simulation Results

In this section we present the simulation results showing the performance of the proposed solutions. First, the error bars for the Monte–Carlo integration method are shown in Fig. 2. Figure 2 indicates that reasonable error values can be obtained with a number of Monte–Carlo samples equal to 500. Fig. 3 shows the dependence of the computing time on the number of Monte–Carlo samples used; the proposed algorithm, with 500 samples, requires slightly more than 1 ms per normalized overlap area evaluation. The simpler GLR statistic requires 0.04 ms per evaluation. Thus the latter looks more attractive from a computational point of view.

The next set of figures explains the behaviour of the Monte–Carlo estimator in the situations when the approximated normalized overlap area and sample size vary. In particular, Fig. 4 shows how Relative Mean Squared Error (RMSE) scales with the normalized area overlap for a fixed Monte–Carlo sample size. Because in this case we consider the ratio of absolute MSE to the square of the true value, the relative error increases as the normalized area of overlap decreases. This implies that the absolute error is approximately constant (see also Fig. 2) and it is stable in the range of interest. To generate this figure we compared the value estimated via Monte–Carlo integration to the normalized overlap area that can be analytically derived for the case when ellipses simplify to circles. Figure 5 shows how MSE scales with Monte–Carlo sample size  $N$  for a

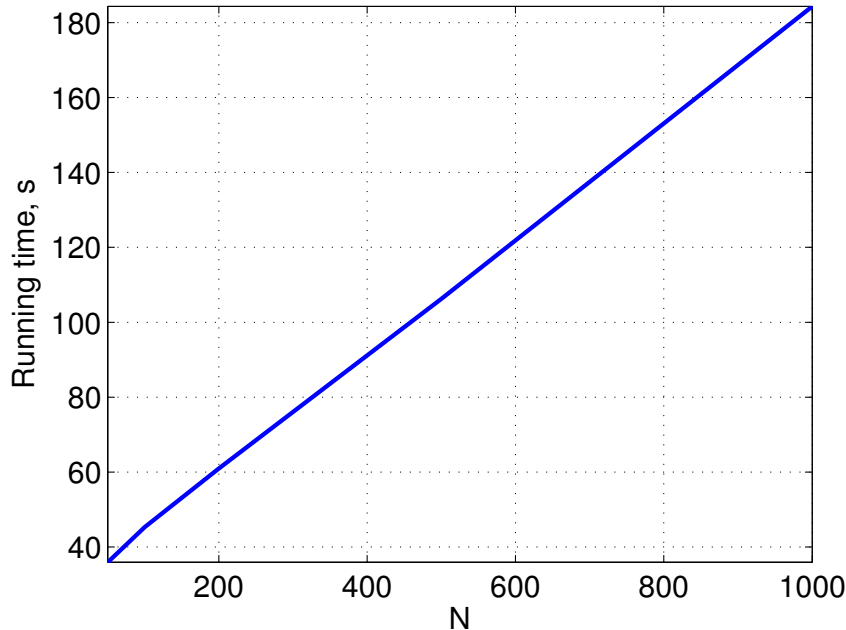


Figure 3. Computing time, as a function of the number of samples,  $N$ , for 100,000 evaluations of the normalized overlap area using the Monte–Carlo algorithm.

fixed overlap area. As expected, the approximation error can be easily controlled by changing the sample size. The doubling of the sample size leads to a 3 dB decrease in the MSE error. Thus the performance of the Monte–Carlo method is a trade-off between the approximation error introduced (see Fig. 5) and the computational effort involved (see Fig. 3).

The last plot, Fig. 6, shows the comparison between the statistics we studied. In particular, in this plot, the thick blue (dark grey) line corresponds to the Monte–Carlo approximation of the normalized overlap area  $g_M$  defined in (55), the black line shows the values of the GLR statistic  $g_G$  defined in (71), the red (light grey) line corresponds to the Monte–Carlo evaluation of the product of the two Gaussian distributions, and the green (lightest grey, horizontal) line shows the threshold setting at 0.5. In this figure we use the Monte–Carlo estimator with  $N = 1000$  as a reference and examine how well this reference can be approximated by the simpler GLR statistic throughout 10,000 random trials. In each trial a random configuration of two ellipses is generated. We can see that the GLR never reaches 0 or 1, even if there is complete overlap or no overlap at all between the ellipses. On the other hand, it is clear that by applying proper thresholding we can force  $g_G$  to zero or one in these regions. Values of the normalized overlap area between 0 and 1 are approximated by the GLR statistic reasonably well, given the modest computational effort involved in the computation of  $g_G$ . Moreover, in general,  $g_G$  tends to overestimate the overlap area in the region  $[0, 0.7]$ .

We know from [9] that acceptance of false track pairs in this particular problem is not penalized as much as the miss of a true, but distant track pair. Thus as an approximation of operator intuition  $g_G$  exhibits desirable properties in the region  $[0, 0.7]$ . On the other hand, in the region  $[0.7, 1]$ ,  $g_G$  underestimates the true normalized overlap area, but it can be seen clearly that it is always greater than the threshold 0.5. From a psychological perspective [9], this threshold is the best borderline between a track pair that is certainly a false match and a pair that should be

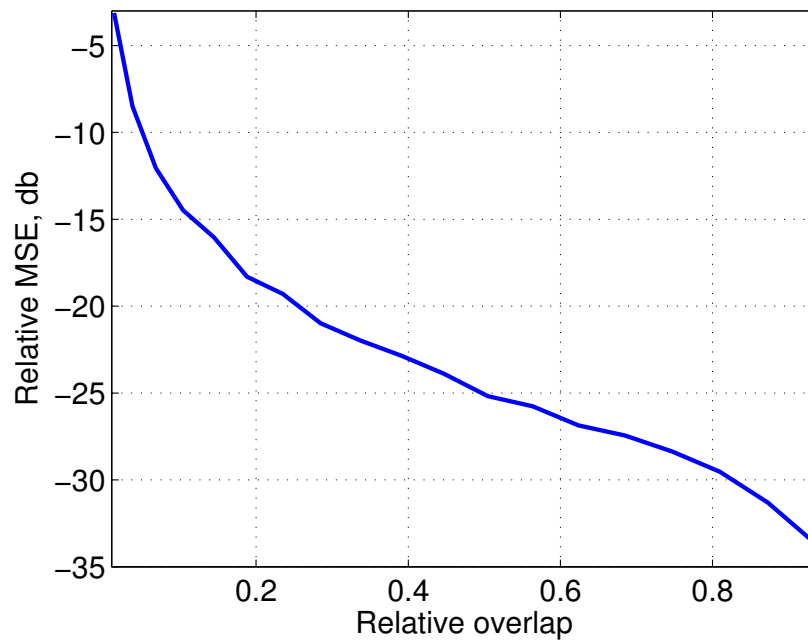


Figure 4. The relative mean-squared error (RMSE) of the Monte–Carlo integration algorithm for the case  $N = 500$ . The absolute mean squared error is the average squared difference between the estimate and the true value. The RMSE is the ratio between this value and the square of the true overlap area. The figure indicates that the RMSE increases as the overlap area decreases, which reflects the desirable property that the absolute mean-squared error remains approximately constant.

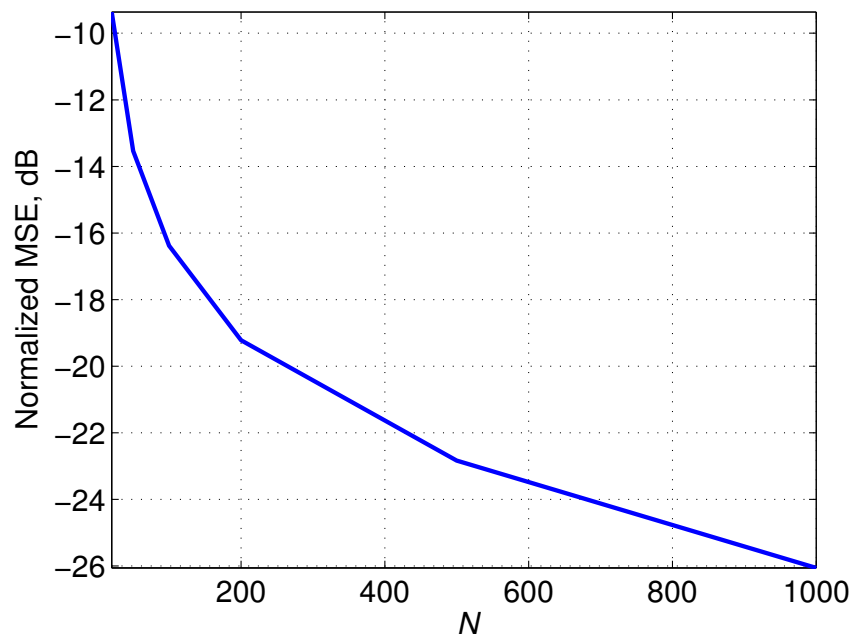
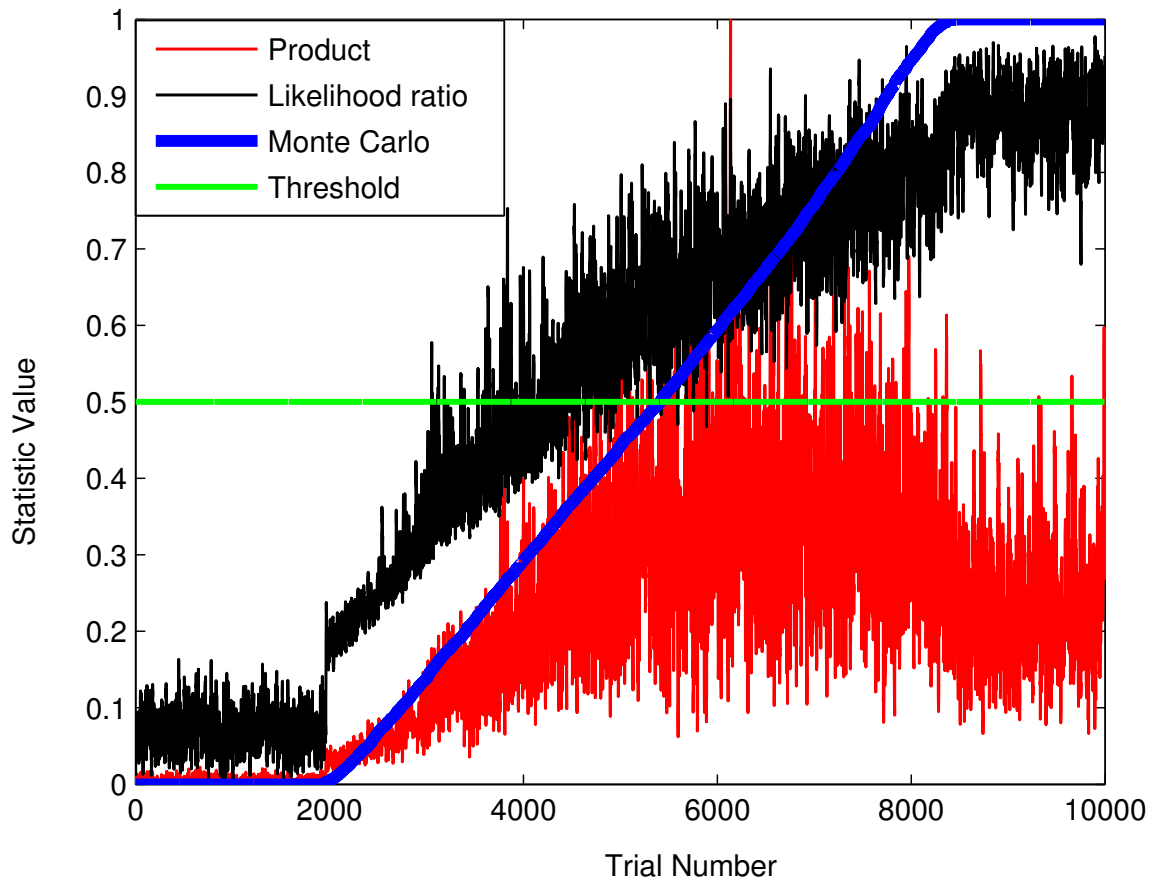


Figure 5. The Monte–Carlo error as a function of the number of samples, for a fixed value of the relative overlap area equal to 0.391.



*Figure 6.* A comparison of statistics over ten thousand trials, each consisting of two random ellipses with varying size, orientation, and overlap. In the figure, trials are sorted in order of the Monte–Carlo estimation of the overlap. The primary comparison is between the Monte–Carlo estimate of the area of overlap and the likelihood ratio statistic. The likelihood ratio is generally slightly larger in magnitude than the Monte–Carlo estimate for relative overlaps between 0 and 0.7, and drops below the estimate for relative overlaps in the range 0.7 to 1.

considered as a potential match. This is also a desirable property. The obvious drawback of the  $g_G$  statistic is that a larger number of track pairs are considered as potential matches as compared with the Monte–Carlo statistic  $g_M$ . In turn this increases the load on the operator who needs to make a final decision regarding the track matching.

#### 4. Conclusions

In this report we focused on the generation of two alternative metrics that can be used to evaluate a geofeasibility score of two tracks. We considered the situation where the only information available for feasibility assessment is geographical information consisting of two  $2\sigma$  ellipses representing the corresponding target position measurements and their uncertainty. The first metric is based on direct evaluation of the normalized intersection area between the two ellipses, based on Monte–Carlo integration. The second metric is based on the GLR statistic under the Gaussian assumption

on measurement uncertainty. The experiments conducted on synthetic data showed the viability of both metrics in terms of the computational burden required to perform numerical calculations and obtain accurate results.

The accuracy and computational resources required for the implementation of the Monte–Carlo based geofeasibility score are easily controlled by varying the Monte–Carlo sample size. Reasonably accurate and fast results can be achieved for sample sizes of 500, requiring slightly more than 100 seconds for 100,000 geofeasibility score evaluations. The GLR based geofeasibility score approximates the normalized intersection area metric reasonably well on average. The computational effort involved in the calculation of the GLR based score is significantly less than that of the Monte–Carlo based score. It amounts to approximately 4 seconds per 100,000 evaluations. The choice between the two proposed metrics depends on the available computational resources, the accuracy required by the application, and the closeness of the metrics to the desired track match indicator.

Although the approach described in this report is, from a mathematical point of view, more satisfying than the geometrical approach, it might not be ideal from a psychological point of view. Recall that the geometrical approach consists of computing the area of intersection of two ellipses. One of the major factors underlying the utilization of a complex and high–criticality system, such as the MUSIC track-to-track fusion system, is the level of trust the operator has in it [4]. Operators may be unwilling to use a reliable automated system leading to high-precision results if they consider it as untrustworthy. An automated system will be trusted to a greater extent if the operators understand the algorithms underlying the system [1]. Maritime surveillance operators perceive AOU as simple two-dimensional ellipses, not as Gaussian distributions, which most of them do not understand. Since operators have to interpret the results, the geofeasibility scoring chosen for the track-to-track fusion system developed within the MUSIC project is a linear approximation of the normalized area of intersection of two ellipses (see the details in [5]). Although this approach may seem too simple from a statistical point of view, it is based on the operator’s perception, arising from many years of field experience.

## References

1. H. Atoyan, J.-R. Duquet, and J.-M. Robert, *Trust in new decision aid systems*, 2006, pp. 115 – 122.
2. A. Doucet, N. de Freitas, and N. Gordon (eds.), *Sequential Monte Carlo Methods in Practice*, Springer–Verlag, Berlin, 2001.
3. Capt. Laurence Hickey, *Background brief — the recognized maritime picture*, Presentation to Senate Committee for National Security and Defence, Canada, Sept./Nov. 2003, available at <http://www.parl.gc.ca/37/2/parlbus/commbus/senate/Com-e/defe-e/witn-e/hickey2-e.htm>.
4. J.D. Lee and K.A. See, *Trust in automation: Designing for appropriate reliance*, **46** (2004), 50–80.
5. E. Lefebvre, C. Helleur, and N. Kashyap, *The use of a multidimensional space for fusion candidate representation in a maritime domain awareness application*, vol. 6974, March 2008.
6. P. C. Mahalanobis, *On the generalised distance in statistics*, Proceedings of the National Institute of Science of India **12** (1936), 49–55.
7. V. H. Poor, *An introduction to signal detection and estimation*, 2 ed., Springer-Verlag, Berlin, 1994.
8. Defense Research and Development Canada, *Multi-Sensor Integration within a Common Operating Environment (MUSIC), Technology Demonstration (TD)*, May 2006.
9. M.-O. St-Hilaire, *Recognized maritime picture — Montreal Industrial Problem Solving Workshop (IPSW) problem statement*, personal communication, August 2007.
10. M.-O. St-Hilaire, E. Lefebvre, and C. Helleur, *Track modeling for maritime surveillance*, Proceedings of 11th International Conference on Information Fusion, July 2008.